Supplementary Materials

David Reens,* Hao Wu,* Tim Langen,† and Jun Ye
JILA, National Institute of Standards and Technology and the University of Colorado and Department of Physics, University of Colorado, Boulder, Colorado 80309-0440, USA
(Dated: September 18, 2017)

The present study on the role of mixed fields for spin-flip loss evolved out of our continuing investigations into the collisional processes reported in Refs. [1, 2]. These investigations have revealed that an important fraction of the effects attributed to collisions are in fact attributable to spin-flip losses. In Sec. A and Sec. B we provide the interested reader with our current best understanding of the situation. Lastly, we provide in Sec. C an algebraic derivation of the loss enhancement factor presented in Eqn. 3 of the main text [3].

A. Electric Field Induced Collisions

We begin with Ref. [1] on electric field induced inelastic collisions. The authors identified the same single particle spin-flip loss enhancement process we discuss [3], and an attempt was made at deconvolution from the collisional effect (App. A, Ref. [1]). Since that time, new observations prompted us to make an even more careful investigation, during which we discovered an important mathematical improvement.

Relative to the approach taken in App. A of Ref. [1], we make the same simplifying assumptions: loss only occurs in the $\vec{E} \perp \vec{B}$ plane, only the velocity orthogonal to this plane matters, and the population is a thermalized Maxwell-Boltzmann distribution. Our correction relates to the next step, where an integral calculation for the loss rate is performed. In Ref. [1] the integration spans the entire 3D spatial distribution, weighted by the frequency of crossing of the center plane and the chance of loss for each crossing:

$$\Gamma_{\mathrm{LZ}} = \int_0^\infty 4\pi r^2\, n(r) dr \int_0^\infty n(v_\theta) dv_\theta \left(\frac{v_\theta}{\pi r} P_{\mathrm{hop}}(r, v_\theta)\right) \quad (1)$$

Here $n(r)$ is the radial distribution function, constrained to satisfy $\int_0^\infty 4\pi r^2 n(r) = 1$, and of the form $n(r) \propto e^{-\mu_B B`r/kT}$. Likewise $n(v_\theta)$ is the usual normalized Maxwellian velocity distribution. Implicit in this integration is the simplifying assumption that molecules at a given radius r cross the center plane with a frequency of $v_\theta/\pi r$. Though not a bad place to start, this approximation is rather rough given that molecules are certainly not following circular orbits of constant v_θ but are in general following some unusual trap motion. Our correction is to perform an integration of flux through the loss plane directly:

$$\Gamma_{\mathrm{LZ}} = \int_0^\infty 2\pi r\, n(r) dr \int_0^\infty n(v_z) dv_z \left(v_z P_{\mathrm{hop}}(r, v_z)\right) \quad (2)$$

Here the same distributions are used, but the spatial distribution is integrated over the central plane only, hence the $2\pi r$ Jacobean, and the hopping probability is multiplied by the velocity v_z to give a flux. The coordinates z and θ are mathematically equivalent in the central plane, but z is more appropriate given that integration is no longer spanning the θ direction. This flux integral gives the desired loss rate without any approximations about molecule orbits or plane-crossing frequency. Although the two integrals differ significantly in their conception, mathematically the changes to the integrand and the Jacobean reduce to precisely an overall scaling factor of π.

The influence of this on the deconvolution procedure relates to the details of the two-body fitting routine. One plus two body fits were performed to various decay trap curves:

$$\dot{N} = -\gamma N - \beta N^2 \quad (3)$$

with the one body component fixed to the value expected due to vacuum scattering and spin-flip loss. An example of such decay curves is shown in Fig. S1(a), where Electric field is turned on suddenly after various hold times. With the stronger spin-flip loss, it is no longer appropriate to assume this loss will be present in the data as a pure one-body decay. Rather, only those molecules whose orbits regularly intersect the loss region are lost, after which thermalization would be required to repopulate the loss prone regions of phase space. If thermalization is slow, spin-flip loss can have a rate that decreases over time, producing a time dependence of population like that of a two-body effect. Even though the possibility of a factor of two error in the calculated magnitude of spin-flip loss was considered in [1] (Fig. S1(b), shaded region), the possibility of its influencing the data in a non-single-particle manner was not considered.

We can perform single particle simulations of spin-flip loss to investigate this, and we obtain curves such as shown above the time dependent experiment data points in Fig. S1(a). We can even perform a two body fitting

* Contributed equally. Email dave.reens@colorado.edu or hao.wu@colorado.edu.
† Present Address: 5. Physikalisches Institut and Center for Integrated Quantum Science and Technology (IQST), Universität Stuttgart, Pfaffenwaldring 57, 70569 Stuttgart, Germany

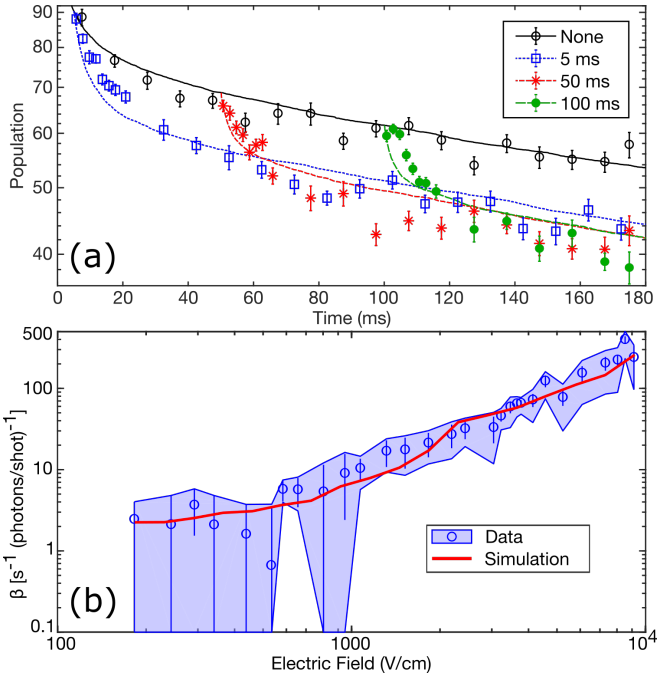

FIG. S1. Experimental electric field induced loss data with an attempted overlap to spin-flip loss simulations. The case of no electric field (black, solid) is compared to electric fields of in 3 kV/cm turned on after a wait time indicated in the legend. (b) Two body fits from [1] to experimental data like that in (a) but at various electric fields. The blue data points and shaded region are repeated from Fig. 3 of [1], where the shading indicates the variation that would be brought about by changes in the single particle effect by a factor of two in either direction. Even though we discover a factor of only three, the spin flip loss simulation (thick red solid line) matches the data within errorbars.

procedure like the one used in [1] to the single particle spin-flip loss simulation traces, see Fig. S1(b). The results suggest that the effect attributed to two-body collisions could be largely explained by spin-flip losses. Still, there are notable differences, such as in the initial rate of the decays in fig. S1(a), which is faster in simulation than in experiment, and in the long time magnitude of the loss, which is maybe 10% larger in experiment than simulation. One avenue to try and be more quantitative would be to incorporate collisions in the simulation and see what collision rates yield the best agreement. Unfortunately there are many challenges in the quantitative application of these simulations, such as uncertainty regarding the initial distribution and the existence of various partially trapped substates. We think the best path forward is to perform future collisional studies with the single-particle effect removed [3].

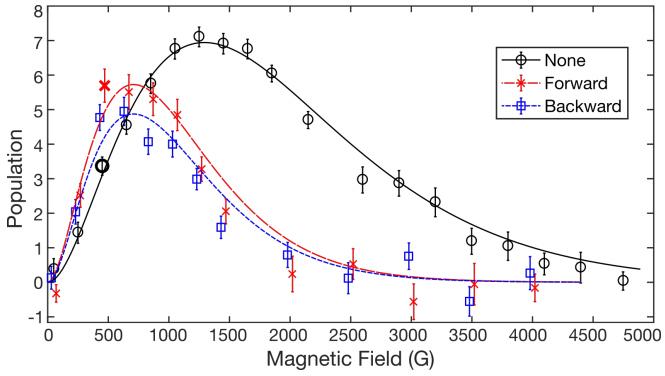

FIG. S2. Normalized spectra are performed under three conditions: one with no evaporation (black circles), one with an exponential RF evaporation ramp over 170 ms (red x's), and a third with this ramp applied in a time reversed manner (blue squares). Solid lines are fits to Maxwell-Boltzmann distributions with temperatures of 59 ± 2 in the case of no evaporation (black), and 30 ± 3 for both forward (red, long dashes) and backward (blue, short dashes) evaporations. The forward evaporation achieves a clear density enhancement in the vicinity of 500 G, where the line markers are bolded.

B. Evaporation

With regard to [2], the present study has important ramifications, since the process of evaporation and depletion spectroscopy required the use of electric fields. Molecules were transferred from positive to negative parity at specific magnetic fields, and subsequently destabilized by the addition of electric field to open avoided crossings. These crossings would only allow molecules above 500 G to escape, so it was thought that a cold population insensitive to the spectroscopic technique was building up at lower fields. Given the existence of spin-flip loss caused by the electric field at the very center of the trap where such a cold population would build up, we reject this hypothesis of a hidden cold population. The cold hidden population hypothesis was essential to the temperature fits performed in Fig. 3 of [2], which are therefore no longer trustworthy.

Nonetheless, without fitting temperatures, it is still possible to use normalized spectra to look for enhancements in density caused by the evaporation. The normalization simply rescales the trace so that the area beneath adds up to the observed total population by laser induced fluorescence. Without it, spectroscopies of smaller populations yield distributions with enclosed areas that are decreased much more than the actual population. We repeatably find such enhancements for evaporation sequences designed to achieve a twofold temperature reduction, see Fig. S2. The initial temperature of 59 ± 2 mK is higher than reported in [2] due to an important correction to the molecular Hamiltonian found by inclusion of nearly one hundred molecular states [4].

Seeking to more thoroughly corroborate this observation in a way that does not depend on normalizations,

we have compared the populations under two related conditions- the first a normal evaporation sequence and the second an evaporation with time-reversed microwave frequency. In other words, the cut goes backwards from deep to shallow. This comparison subjects all molecules to the same integrated microwave power, and thus the two conditions should be equivalent in a situation with only single particle effects. However, with respect to collisional effects, the time-reversed case functions like a truncation, preventing molecules that would otherwise have collisionally thermalized to lower temperatures from doing so. To whatever extent an evaporation is successful in facilitating beneficial thermalizing collisions, the time-reversed condition should perform worse. We consistently observe higher final numbers from the forward sequence, at about the 5% level. One possible caveat would be the existence of very slow single-particle shelving processes where molecules slowly leak into some state that is sensitive to the detection laser but not the microwave knife. This would result in the forward evaporation yielding higher final numbers by purely single particle means, but no fully plausible processes have been identified. For example, electric field induced spin-flip loss could allow the well-trapped $|f, 3/2\rangle$ molecules to slowly leak into $|f, 1/2\rangle$, and the latter does have a different behavior with respect to microwave spectroscopy. But the electric fields also ought to destabilize these molecules and prevent them from staying in the trap in either case.

More recently, we have developed the ability to reduce population without perturbing phase space distribution, mentioned and used to look for collisions in [3]. This is non-trivial, and many possible techniques have key drawbacks. For example it is not possible to change the discharge yield of OH in our supersonic expansion without also influencing the temperature of the initial distribution, which is effected by the discharge. We opt for the application of microwaves during deceleration to couple weak and strong field seeking states at low magnitudes of electric fields experienced by all molecules when flying through a de-energized stage just after switching. The microwaves are applied via microwave horn and have a long wavelength relative to the cloud, so that microwave power variations across the cloud are not relevant. The microwaves are applied early during deceleration, so that the molecules have many stages of deceleration and the process of trap-loading left to remix any asymmetries in the removal process. It is difficult to experimentally verify that the phase space distribution function is truly unaffected in all six dimensions, but in at least one dimension, the time of flight profile of slowed molecules after deceleration, the distribution is unaffected even by tenfold reductions using this technique.

In conclusion, the role of collisional effects in Ref. [1] is reduced by spin-flip losses, but spectroscopic comparisons and evaporation subtractions still point to an evaporative effect. The development of various more sensitive tools has us poised to more unambiguously identify any future collisional effects in our next generation system.

C. Scaling Law Derivation

Here we derive the loss enhancement scaling law presented in Eqn. 3 of the main text [3], and repeated here:

$$\eta \propto \left(\frac{d_{\rm eff}E}{\sqrt{\kappa\Delta}}\right)^{8/3}. \tag{4}$$

The key idea is to compare the surface areas of the loss regions with and without electric field. There is no exact loss region where a molecule is guaranteed to hop, but rather its velocity and direction contribute to the Landau-Zener probability (Eqn. 2, Ref. [3]). Nonetheless, for the purposes of a scaling law, we can assume the average thermal velocity v_T, and choose a probability threshold of $P > 1/e$. These assumptions allow us to define the loss region as the contour surface of energy κ where

$$\kappa = \sqrt{\hbar\dot{G}} = \sqrt{2\hbar v_T B'}; \tag{5}$$

G is the energy gap between the trapped state and its spin flip partner, and B' is the trap gradient.

One complication is that in a quadrupole trap there is a weak and a strong axis, so that B' varies by as much as a factor of two in different directions. We assume that the electric field is applied parallel to the strong axis, which leads to a loss plane where $\vec{E} \perp \vec{B}$ perpendicular to the strong axis. This matches the geometry that has been realized in our experiment [1], and is the worst case, but by no more than a constant factor of $2\sqrt{2}$ relative to other directions the electric field could have. We always use B' to refer to the stronger gradient.

Before application of electric field, the κ valued energy contour is an oblate ellipsoid of long radius $r_0 = 2\kappa/\mu_{\rm eff}B'$. Its area is then $2\pi \cdot 1.38 r_0^2$, where the prefactor comes from the specific $2:1$ aspect ratio of the ellipsoid and is hereafter neglected. When electric field is applied, the energy gap near the trap zero takes the following functional form:

$$G(r,z) = \mu_{\rm eff}B'|z| + \alpha(\mu_{\rm eff}B'r/2)^3\frac{\Delta\sqrt{\beta\Delta^2 + d_{\rm eff}^2E^2}}{(d_{\rm eff}E)^4}, \tag{6}$$

plus higher order terms in r and z. Here we use r to denote the in-loss-plane coordinate and z to denote distance away from the loss plane, along the strong axis of the trap. The constants α and β are nearly unity for OH and will be ignored henceforth. This is essentially Eqn. 1 of Ref. [3] but with an explicit coordinate system, and can be derived by series expanding the energy difference between the trapped state and its spin-flip-partner. The energy difference can be derived for OH by diagonalizing the ground state hamiltonian in mixed fields, see App. A of Ref. [5], or similarly for any other species.

Now we use Eqn. 5 to compute the area of the surface $G = \kappa$. We specialize to the regime where $d_{\rm eff}E < \Delta$, so that $\Delta \approx \sqrt{\Delta^2 + d_{\rm eff}^2E^2}$. For larger fields, one Δ can

be exchanged for $d_{\text{eff}}E$, but in practice the loss rate is already so high in these regimes that no sample remains trapped. The radial extent of the surface can be solved by inverting $\kappa = G(r, 0)$:

$$r_E = \frac{1}{\mu_{\text{eff}}B'} \sqrt[3]{\frac{8\kappa(d_{\text{eff}}E)^4}{\Delta^2}}. \tag{7}$$

The axial extent remains $z = \kappa/\mu_{\text{eff}}B'$ for all $\vec{E}$. For large enough E, r_E dominates over this axial extent, so that the area is effectively $2\pi r_E^2$ and the loss area enhancement becomes $\eta = (r_E/r_0)^2$. Comparing the expressions for r_E and r_0, $\mu_{\text{eff}}B'$ cancels and we have

$$\eta = \left(\frac{1}{2\kappa} \sqrt[3]{\frac{8\kappa(d_{\text{eff}}E)^4}{\Delta^2}} \right)^2 = \left(\frac{d_{\text{eff}}E}{\sqrt{\kappa\Delta}} \right)^{8/3}. \tag{8}$$

Now we address the domain of validity of this result. When E is small, Eqn. 5 only has a narrow range of validity, since the electric field only dominates in a very small region near the trap center. Outside, G retains a nearly linear dependence on r. This means that Eqn. 6 only holds for E above some threshold. For smaller E, r_E will simply not be significantly perturbed from its zero electric field value of $r_0 = 2\kappa/\mu_{\text{eff}}B'$. The implication for the enhancement factor in Eqn. 7 is simply that it is only valid when it predicts an enhancement significantly greater than unity. In other words, Eqn. 7 holds when $d_{\text{eff}}E > \sqrt{\kappa\Delta}$, but below this η just gradually returns to unity. Eventually when $d_{\text{eff}}E > \Delta$, $\eta \propto (d_{\text{eff}}E)^2$ instead of 8/3, and by this point the enhancement η is already greater than Δ/κ, generally a very large factor.

[1] B. K. Stuhl, M. Yeo, M. T. Hummon, and J. Ye, Molecular Physics **111**, 1798 (2013).

[2] B. K. Stuhl, M. T. Hummon, M. Yeo, G. Quéméner, J. L. Bohn, and J. Ye, Nature **492**, 396 (2012).

[3] See Main Text.

[4] K. Maeda, M. L. Wall, and L. D. Carr, New Journal of Physics **17**, 45014 (2015).

[5] B. K. Stuhl, M. Yeo, B. C. Sawyer, M. T. Hummon, and J. Ye, Physical Review A **85**, 033427 (2012).